Kalahari 008, 009

Anorthositic regolith / basaltic fragmental breccias
598, 13500 g

Figure 1: Kalahari 009 with a 1 cm scale cube (photo courtesy of A. Bischoff).

Introduction

Kalahari 008 and 009 (Fig. 1) were found in September 1999, in Botswana, in front of a sand dune in the Kalahari desert (Fig. 2). Kalahari 008 is a feldspathic regolith breccia (Fig. 3a) and Kalahari 009 is a fragmental basaltic breccia (Fig. 3b). These meteorites are very different in lithology, but are proposed to be paired due to their close find proximity, very short cosmic ray exposure ages, fayalitic olivine, and possibility that they could form in a lunar setting (Sokol and Bischoff, 2005a,b; Russell et al., 2005).

Figure 2: Region of Botswana in which Kalahari 008 and 009 were found.

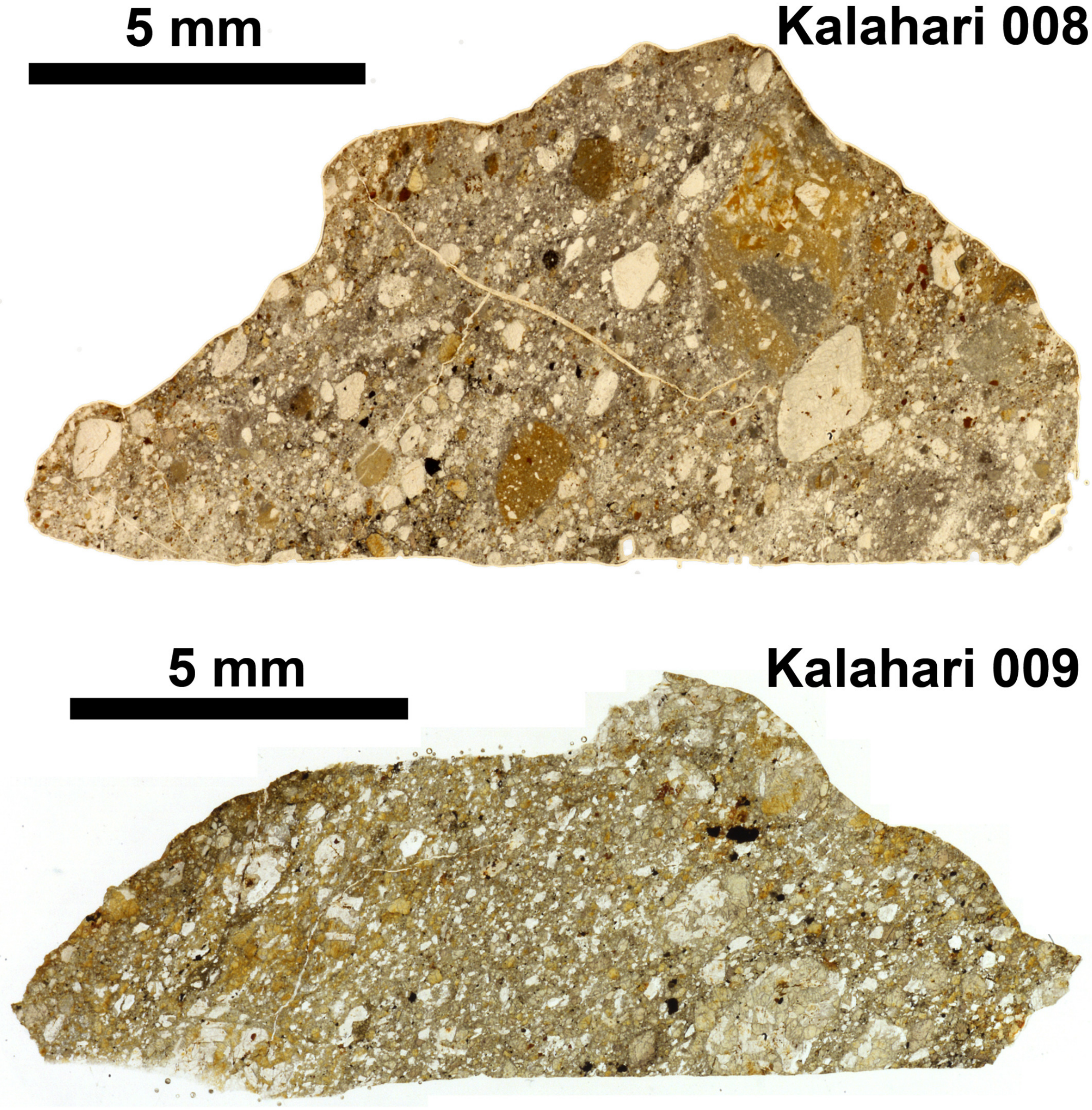

Figure 3: Plane polarized light images of thin section of Kalahari 008 (a) and 009 (b) (photos courtesy of A. Bischoff).

Petrography and mineralogy

Kalahari 008 contains feldspathic impact melt breccias, granulitic breccias, and cataclastic anorthosites (Sokol and Bischoff, 2005). This meteorite also contains solar wind implanted gases (Russell et al., 2005), and glassy spherules (Fig. 4a) consistent with a regolith origin. Plagioclase feldspars are An_{86} to An_{99} in composition (Fig. 5), and olivines are Fa_{28} to Fa_{98} (Fig. 6). The impact melt clasts are similar in composition to Apollo 16 impact melt breccias (Cohen, 2005).

Kalahari 009 is a fragmental basaltic breccia containing various basaltic clasts (Fig. 4b) in a fine grained matrix (Sokol and Bischoff, 2005b). Dominant phases in this sample are pyroxene, plagioclase, and olivine. Some of the pyroxenes have fine exsolution lamellae. Minor and accessory phases include ilmenite, chromite, troilite, ulvospinel, and FeNi metal. A common occurrence of silica-hedenbergite-fayalite intergrowths is attributed to the breakdown of pyroxferrite (Fig. 4c; Sokol and Bischoff, 2005b). Plagioclase feldspars are largely An_{88} to An_{96} in composition (Fig. 5), and olivines are Fa_{52} to Fa_{99} (Fig. 6). Pyroxenes in clasts and fragments very in composition out to ferro-augites, similar to pyroxenes in Apollo 12 and 15 rocks (Fig. 7; Papike et al., 1976). There are no solar wind gases detected in this meteorite, as opposed to Kalahari 008 (Russell et al., 2005).

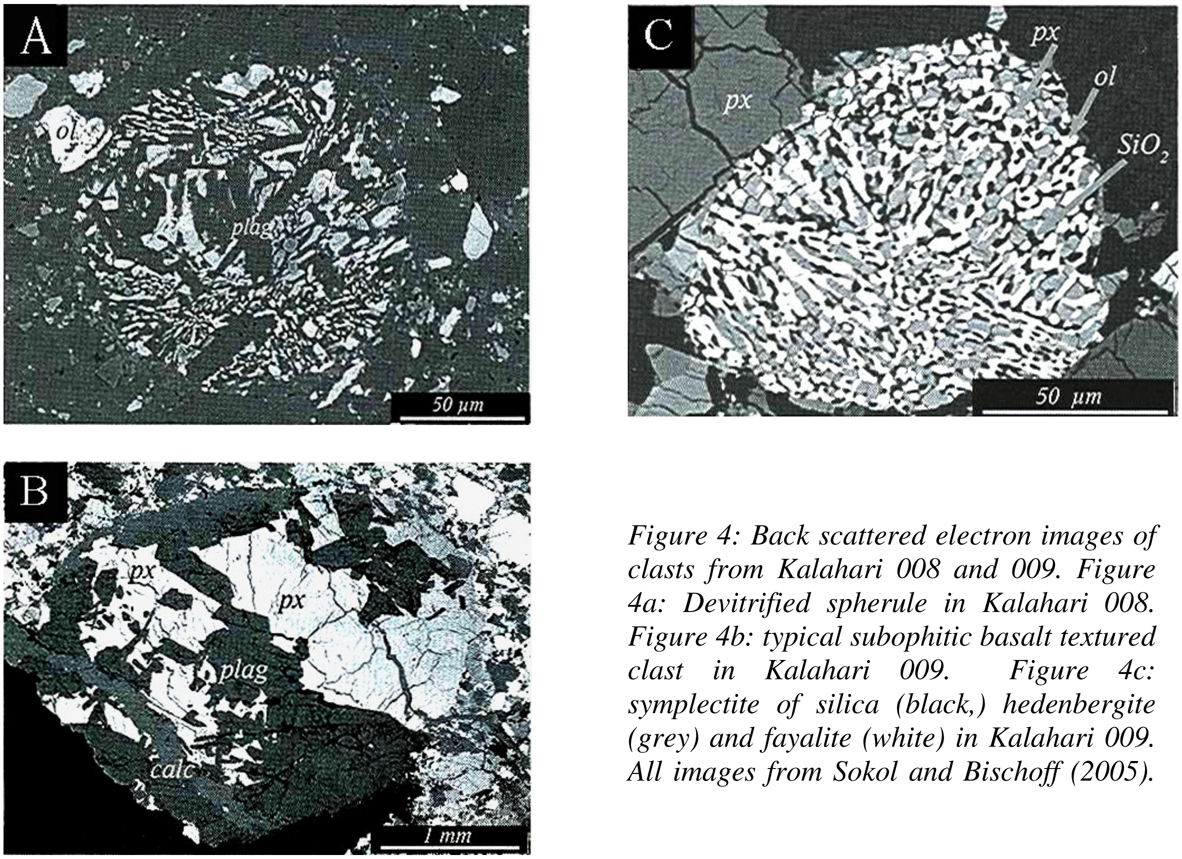

Figure 4: Back scattered electron images of clasts from Kalahari 008 and 009. Figure 4a: Devitrified spherule in Kalahari 008. Figure 4b: typical subophitic basalt textured clast in Kalahari 009. Figure 4c: symplectite of silica (black,) hedenbergite (grey) and fayalite (white) in Kalahari 009. All images from Sokol and Bischoff (2005).

Chemistry

The bulk composition of Kalahari 008 is typical of many feldspathic lunar meteorites with 4.7% FeO and 0.75 ppm Sm (Korotev et al., 2008). Kalahari 009 has more unusual composition for a basaltic meteorite with low FeO, TiO_2, incompatible elements, and trivalent REE (Korotev et al., 2008; Schulz et al., 2007).

Radiogenic age dating

Initial age dating for Kalahari 009 was done using the ^{39}Ar-^{40}Ar approach (Fig. 8; Fernandes et al., 2006). Although the lower temperature part of the spectrum appears to be disturbed, the higher temperature fractions (>0.6) indicate an age as old as 2.7 Ga, but ranging down to 1.7 Ga (Fernandes et al., 2007a, b). Dating of phosphates using U-Pb and ion microprobe analysis results in a much older age of 4.35 ± 0.10 Ga (Fig. 9; Terada et al., 2007). These older ages are supported by a Lu-Hf isochron of ~4.2 Ga (Schulz et al., 2007) as well as Rb-Sr and Sm-Nd ages of 4.30 ± 0.05 Ga (Fig. 10; Shih et al., 2008). These older ages suggest that the Ar ages reflect resetting from a younger impact event (e.g., Fernandes et al., 2007b). The Sr and Nd isotopic results suggest a connection between the Kalahari 009 VLT basalt and aluminous mare basalt from Apollo 14 (Fig. 11; Shih et al., 2008). Additionally, ages of impact melt clasts in the feldspathic Kalahari 008 have been measured in two samples, yielding 2.05 and 2.08 Ga (Cohen, 2008).

Cosmogenic isotopes and exposure ages

One of the most distinctive features of this meteorite pairs is their very short exposure ages. Nishiizumi et al. (2005) measured an Earth-Moon transit time of 230 ± 90 yr. An age this young might indicate a non meteoritic age, but the ^{36}Cl content is higher than that which would be expected for in situ production from a terrestrial sample; the excess ^{36}Cl must have been produced in space (Nishiizumi et al., 2005).

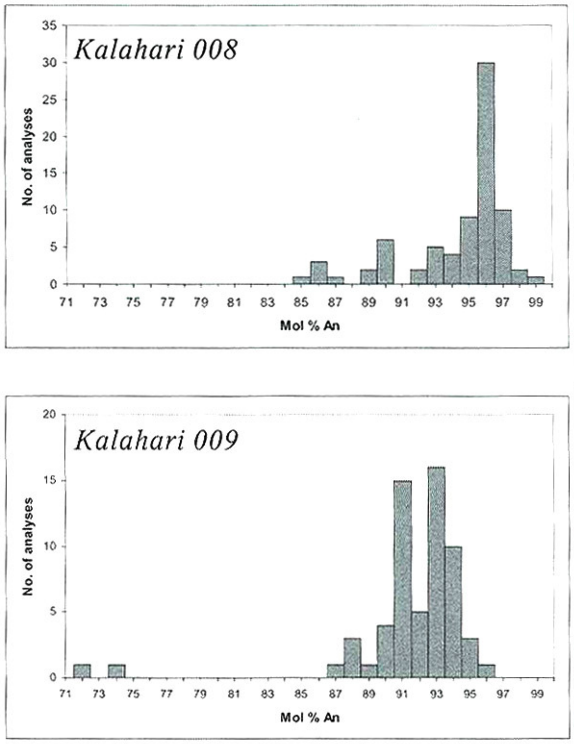

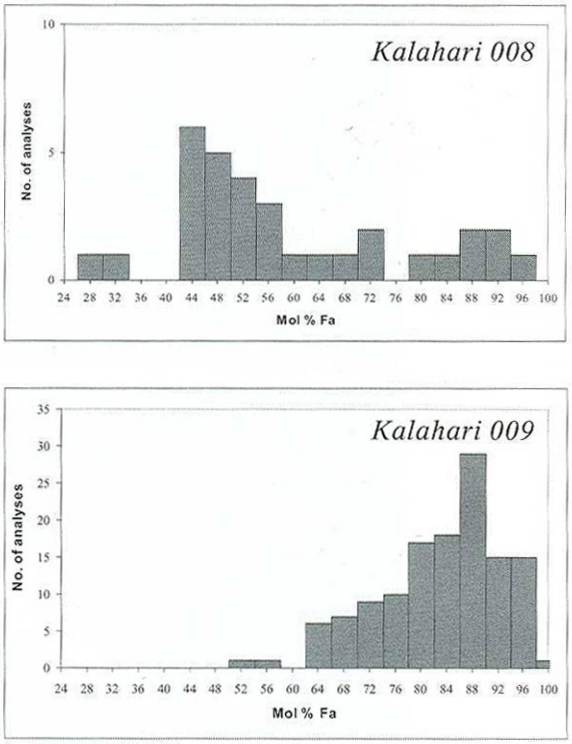

Figure 5: Plagioclase feldspar compositions in Kalahari 008 and 009 (from Sokol and Bischoff, 2005). Figure 6: Olivine compositions in Kalahari 008 and 009 (from Sokol and Bischoff, 2005).

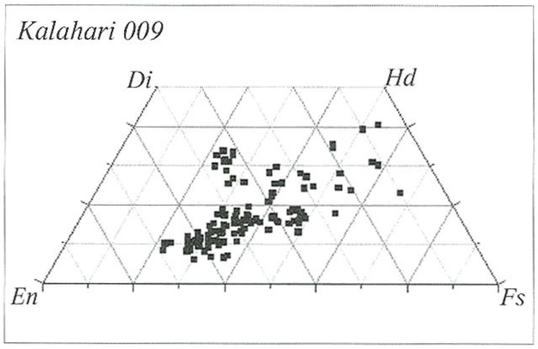

Figure 7: Pyroxene compositions from Kalahari 009 (from Sokol and Bischoff, 2005).

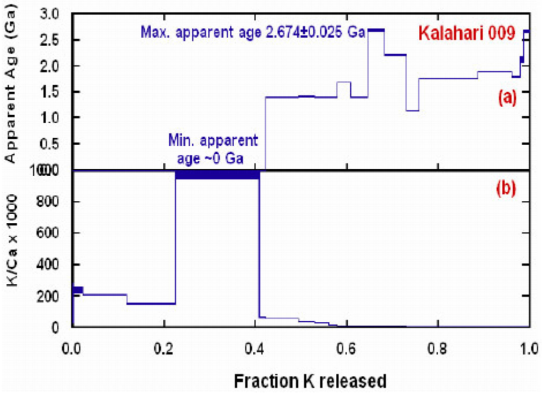

Figure 8: ^{39}Ar-^{40}Ar spectrum for Kalahari 009 (from Fernandes et al., 2006). Although the lower temperature part of the spectrum appears to be disturbed, the higher temperature fractions (>0.6) indicate an age as old as 2.67 Ga.

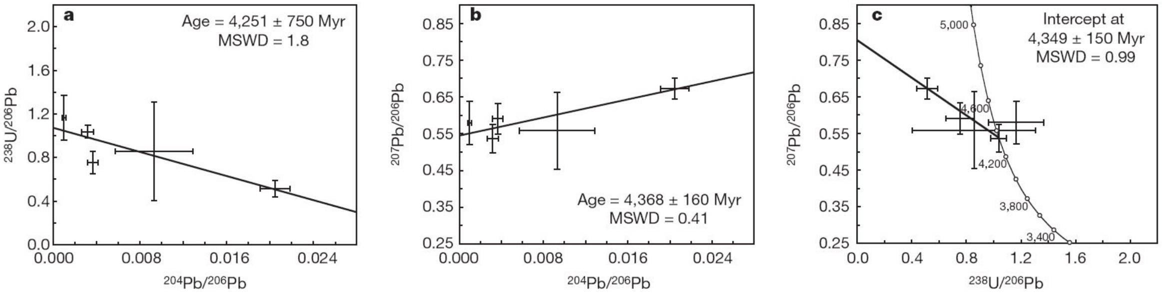

Figure 9: Results of U-Pb dating of phosphates in Kalahari 009, in an inverse U-Pb (a), inverse Pb-Pb (b) and projection in three dimensional space of the total Pb isochron (from Terada et al., 2007).

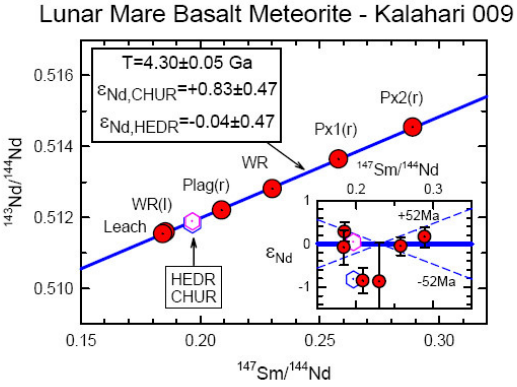

Figure 10: ^{147}Sm-^{143}Nd isochron for Kalahari 009 (from Shih et al., 2008), yielding an age of 4.30 Ga.

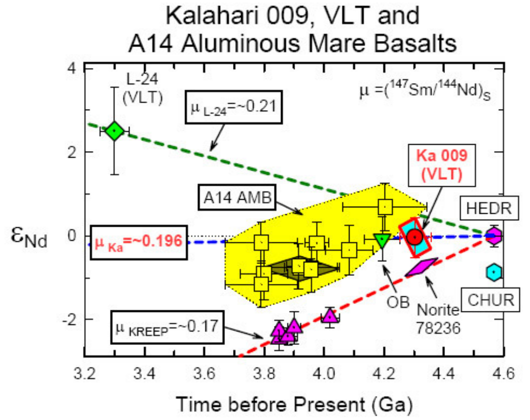

Figure 11: Epsilon Nd versus time for Kalahari 009 samples showing the nearly chondritic Sm/Nd at 4.3 Ga, similar to Apollo 14 aluminous mare basalt (from Shih et al., 2008).

Table 1. Chemical composition of Kalahari 008 and 009

reference	1 (009)	2 (009)	2 (008)
weight	?	265	278
technique	a,b	a	a
SiO_2 %	46.04		
TiO_2	0.67		
Al_2O_3	12.70		
FeO	18.50	16.4	4.67
MnO	0.23		
MgO	7.88		
CaO	11.17		
Na_2O	0.44	0.485	0.561
K_2O	0.19		
P_2O_5	0.02		
S %			
sum			
Sc ppm	45	53.2	10.9
V	143		
Cr	2500	2880	710
Co	23.3		
Ni	<20	<150	60
Cu			
Zn			
Ga	1.0		
Ge			
As	0.4		
Se			
Rb			
Sr			
Y			
Zr			
Nb			
Mo			
Ru			
Rh			
Pd ppb			
Ag ppb			
Cd ppb			
In ppb			
Sn ppb			
Sb ppb			
Te ppb			
Cs ppm			
Ba			
La	0.94		
Ce	3.7		
Pr			
Nd	3.4		
Sm	0.74	0.603	0.747
Eu	0.4	0.479	1.014
Gd	2.0		

Tb	0.2		
Dy	4.0		
Ho	0.36		
Er	<9		
Tm	<0.3		
Yb	1.6		
Lu	0.3		
Hf	0.7		
Ta	0.1		
W ppb	300		
Re ppb	30		
Os ppb			
Ir ppb	<4		
Pt ppb			
Au ppb			
Th ppm	0.10	0.06	0.17
U ppm	0.14		

technique (a) INAA, (b) XRF

References: 1) Schulz et al. (2007); 2) Korotev et al. (2008).